

## Article

# The Experimental and FEM Studies of Friction Welding Process of Tungsten Heavy Alloy with Aluminium Alloy

Radosław Winiczenko <sup>1,\*</sup>, Andrzej Skibicki <sup>2</sup> and Paweł Skoczylas <sup>3</sup> 

<sup>1</sup> Institute of Mechanical Engineering, Warsaw University of Life Sciences, Nowoursynowska 166, 02-787 Warsaw, Poland

<sup>2</sup> Faculty of Mechanical Engineering, Bydgoszcz University of Science and Technology, Kaliskiego 7, 85-789 Bydgoszcz, Poland; andrzej.skibicki@pbs.edu.pl

<sup>3</sup> Institute of Mechanics and Printing, Warsaw University of Technology, 02-524 Warsaw, Poland; pawel.skoczylas@pw.edu.pl

\* Correspondence: radoslaw\_winiczenko@sggw.edu.pl

**Abstract:** Experimental and finite element studies of the rotary friction welding (RFW) process of tungsten heavy alloy (THA) with aluminium alloy 5XXX series are presented. A 2.5D torsion simulation model including the circumferential effects was developed in this study. The temperature distributions, effective stress, flash dimensions and axial shortening were calculated on un-rotated friction welding aluminium parts. The peak temperatures were measured both in the axis and at the half-radius of the specimen. The maximum interface temperature of 581 °C for the friction weld was below the melting temperature of the aluminium alloy. The experimental and numerical results of the temperature and final weld geometries show good agreement between them. The results indicate very small deviations of 4.45%, 2.96%, and 2.34% on the flash width, flash height and axial shortening of friction welds.

**Keywords:** friction welding; tungsten heavy alloy; FEM



**Citation:** Winiczenko, R.; Skibicki, A.; Skoczylas, P. The Experimental and FEM Studies of Friction Welding Process of Tungsten Heavy Alloy with Aluminium Alloy. *Appl. Sci.* **2024**, *14*, 2038. <https://doi.org/10.3390/app14052038>

Academic Editors: Gustavo H. S. F. L. Carvalho, Rui Manuel Leal and Ivan Galvão

Received: 29 December 2023

Revised: 2 February 2024

Accepted: 21 February 2024

Published: 29 February 2024



**Copyright:** © 2024 by the authors. Licensee MDPI, Basel, Switzerland. This article is an open access article distributed under the terms and conditions of the Creative Commons Attribution (CC BY) license (<https://creativecommons.org/licenses/by/4.0/>).

## 1. Introduction

Friction welding is a joining method that enables the relatively quick and cheap joining of various metals. The physical process of friction welding involves using mechanical energy and converting it into heat, as a result of friction on the contact surface. Friction welding is a solid-state welding method for different metals [1]. The material to be welded is heated to a temperature below its melting point. After stopping the spindle rotation, the joint is pressed and plasticized. As a result of the applied upsetting force, the material is removed to the outside where a flash weld is formed [2]. The friction welding process is a heat-activated process that causes the deformation of the welded material and a large temperature gradient in the heat-affected zone (HAZ). Moreover, large effective stresses are generated in the joint and the microstructural changes as a result of high temperatures at the interface [3].

The basic welding parameters in the direct-drive friction welding process are the rotational speed (RS), friction pressure (FP), upsetting pressure (UP), friction time (FT) and upsetting time (UT). The rotational speed is related to the material to be welded and the diameter of the specimens. The rotational speed also determines the heating rate at the interface. Increasing the rotational speed might lead to the softening of the material, a greater extent of recrystallisation, or even increased intermetallic formation. The maximum temperature in the joint during frictional heating depends not only on the pressure but also on the temperature gradient, which depends on the rotational speed in particular [2]. In rotary friction welding, heat is generated by friction, which results in the significant plasticization of the material. The friction pressure as well as subsequent upsetting during rotary friction welding cause changes in the microstructure of the joint

and its surroundings, which can be compared with the changes caused by hot plastic working. A high temperature in some situations, especially when the process lasts longer, enables diffusion across the interface, resulting in a change in the chemical composition in the joint area. The parameters are selected depending on the type of materials to be welded. The friction pressure affects the heating rate of the HAZ. The greater the friction pressure, the higher the rate of plastic deformation in the welded materials and the higher the heating rate in the contact area. The friction time is set in close correlation with the friction pressure and rotational speed. This should ensure an optimal heating speed and the minimal shortening of the welded elements. The friction time is largely influenced by the thermal conductivity of the welded material. During the friction process, the greatest amount of heat is released around the circumference of the friction surface, where the metal achieves the greatest plasticity. The center of the friction surface is heated due to heat conduction. The larger the diameter and the lower the thermal conductivity of the metal, the lower the temperature at the center of the friction surface. The friction time should be selected so that the temperature is equalized over the entire friction surface. The upsetting pressure and time are parameters that mainly affect the quality of the joining materials. In rotary friction welding, the control of the peak and equilibrium torque levels are considered to be crucial for a sound weld. The axial pressure applied during friction welding will affect the rate of shortening (upset), which is usually constant during the equilibrium torque period. Moreover, the 'upset' can be linearly proportional to the axial pressure [3].

Many works have been dedicated to the thermomechanical processes that occur during friction welding. These thermal phenomena have most often been solved using a finite element method (FEM). Thermo-physical data and the material constants of plastic deformation are necessary for the modelling of the welding process.

The first extensive analysis of the conventional friction welding process was conducted in references [4,5]. The temperature distribution and uniform heat flow in the friction welding process of carbon steel bars with a constant friction coefficient and thermal properties were presented. The first numerical analysis of the friction welding process using the finite differences method was carried out by the authors of papers [6,7]. The authors analyzed the time-varying heat input, axial shortening and plastic deformation of welding materials. A two-dimensional finite-difference model for conducting simulations of the temperature fields of the friction welding process was also developed in references [8,9]. The results show a visible difference in the temperature distribution between the conventional and inertia friction welding (IFW) methods. The friction welding of steel bars with identical properties using the finite element method, along with the conditions of element contacts, was proposed in references [10,11]. Moreover, the temperature distribution and final shape of the welds were determined in references [12,13]. A thermo-mechanical finite element model of IFW of two bars as a viscoplastic material was proposed in reference [14]. The FEM model considered the plastic deformation of the joined workpiece and a heat flow analysis was conducted [15]. The effective stress, strain and temperature field for nickel-based alloy friction welded joints were determined. An FEM simulation of the IFW of materials with different physical properties that assumed mechanical and thermal dependencies and the elastic-viscoplastic behavior of the material was completed [16]. A new friction law for the modelling of the continuous drive friction welding (CDFW) of steel was proposed [17]. A FEM method for the friction welding of ceramic-metal [18] and refractory metals [19] was also used. The numerical model for a steady-state flow and the analysis of a coupled thermo-mechanical problem in friction welding was presented [20]. An investigation of the temperature distribution, axial shortening, flash formation and microstructure using inverse heat flow analysis can be found in reference [21].

Due to its high density, high strength, good toughness and other excellent properties, tungsten heavy alloy material has become the first choice for many kinds of kinetic energy armor-piercing bullets. Tungsten alloy penetrator bullets have a high penetration ability thanks to the high-density tungsten alloy, which makes the projectile fly at high speed and with high energy. Recently, tungsten heavy alloy projectile cores have been used as

kinetic energy penetrators (KEPs) for sub-caliber bullets. These THA cores can be joined to a ballistic cap made of an aluminum alloy. This cap protects the projectile against ricochets when it hits the armor plate. These materials are often joined by threads, which require milling. This is problematic because tungsten is difficult to cut due to its relatively high hardness and strength. Therefore, the authors of references [22,23] have proposed the friction welding method for joining these materials. Friction welding is an effective solid-state joining method for various materials.

Compared to the conventional joining method, rotary friction welding is a simple, cheap and very fast process. Moreover, it makes it possible to join metals and alloys that are very difficult to join or are not joinable at all using other methods. This is why friction welding is a very attractive method and is studied in many laboratories across the world. However, there are some difficulties in joining dissimilar materials. These difficulties are caused by very different melting points, different thermal expansion coefficients, the forming of hard precipitates that are usually intermetallic phases, or problems caused by difficulties in the reaching of an appropriate temperature. To overcome these problems, many experimental works have been performed, especially for the joining of aluminum alloys with a stainless steel or tungsten composite.

The friction welding of THA with AA appears to be difficult due to their thermal properties and differing deformability characteristics [22,23]. When estimating the thermal field, a flash dimension and upset (axial shortening) in a friction-welded joint between these materials makes it much easier to control the welding parameters by reducing the number of necessary experiments. This work aims to develop a thermomechanical model using the finite element method to simulate the CDFW of a composite alloy with an aluminum alloy.

## 2. Methodology

### 2.1. Materials

Tungsten heavy alloy THA (Laboratory of Heavy Alloys, Institute of Mechanics and Printing, WUT, Warsaw, Poland) and aluminum alloy 5XXX series were used for the friction welding process. A commercial 5XXX series (AlMg3Mn)-type non-heat treatable wrought aluminum alloy and conventional W-Ni-Fe type tungsten heavy alloy (THA), with a typical 7:3 nickel to iron ratio, were selected for this study. The aluminum alloy used in this study was a cold-worked rod 20 mm in diameter. The tungsten heavy alloy was prepared by mixing the appropriate amount of powder, compacting it, and then using the liquid phase sintering (LPS) method. The method of producing the W-Ni-Fe alloy and aluminum rod is described in reference [23]. Because of the powder metallurgy method used for THA preparation, its microstructure consists of 30–40  $\mu\text{m}$  tungsten grains embedded in a Ni(W, Fe) matrix. The chemical composition and properties of the joined materials are presented in Table 1.

**Table 1.** The properties of the materials used.

Chemical composition							
Material	Al	W	Fe	Ni	Mg	Mn	Si
THA	-	Bal.	2.25	5.25	-	-	-
AA	Bal.	-	0.194	0.002	2.95	0.265	0.1
Mechanical properties							
Material	Tensile Strength (MPa)		Yield strength (MPa)		Elongation (%)		Hardness (HB)
THA	960		680		27		285
AA	276		207		22		83

## 2.2. Experimental Procedure

A rotary drive friction welding machine (ZT4-13 type, ASPA, Wrocław, Poland) with the experimental setup of thermocouples shown in Figure 1 was used to produce a friction weld. Friction welding was achieved for the following parameters: friction force (FF = 12.5 kN), upsetting force (UF = 50 kN), friction time (FT) and upsetting time (UT) of 9.5 s and 6 s. The rotational speed was kept at a constant level of 1450 rpm. The simulations were performed for joints that showed the highest tensile strength of 232 MPa. The thermocouples (TP203K1b2001 type, 'Czaki Thermos-Product', Raszyn, Poland) with a diameter of approximately 1.2 mm were used to study the temperature distribution in the joint. Figure 1a shows a diagram of the arrangement of thermocouples in a non-rotating aluminum sample during welding. Figure 1b shows the measurement positions 1,2,3 for  $\frac{1}{2}$  R of the sample and 4,5,6 for the axis sample. These were located at a distance of 20, 25 and 30 mm from the weld interface. Temperature measurements were performed using the UT325 LCD digital recorder, Uni-Trend Technology, Dongguan City, Guangdong Province, China.

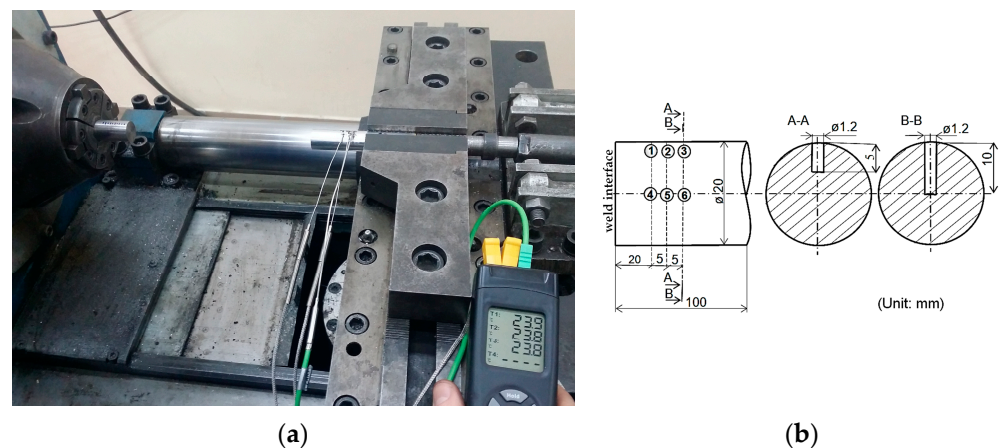


**Figure 1.** Friction welding machine showing placed samples with thermocouple (a), and temperature measurement scheme (b) where: 1,2,3,4,5,6 are the thermocouples positions.

## 2.3. Numerical Procedure

The CDFW model was developed using the commercial finite element (FE) modeling software package, DEFORM 11.0. The software is especially capable of solving problems involving a large plastic deformation via remeshing [24]. The geometry and meshing of the FE model are shown in Figure 2.

A two-dimensional analysis of one-half of the solid element was employed because of the axisymmetric shape of the specimen (Figure 2a). The mesh contained 2125 elements and 2321 nodes (Figure 2b). The dimensions of the modelled parts are consistent with the experiment in terms of width. Three different mesh-sized windows were used. Coarse elements of 0.03 mm were used in the region containing the weld interface. Outside this region, as the distance increases, the element size also increases, and a mesh size of 0.1 mm was used across the model. The effect of the mesh size was also considered in the study. Finally, the mesh size was selected so as not to generate long calculation times. Automatic remeshing was used to maintain a good mesh quality. Many various simulation methods, such as 2D axial-symmetric, 3D full simulation and 2.5D torsion approaches, were initially tested. Finally, a 2.5D torsion simulation including the circumferential effects was accepted for use in this study. A 2.5D model includes all the circumferential velocities needed to account for the torsional friction during welding. In the 2D axial-symmetric approach, the DEFORM code is not able to simulate a rotational speed, and the related shear deformation cannot be computed. The computing time required for a 3D full simulation is very long. In this paper, the torsional friction model has a significant impact not only on heat generation, but also on the deformation of the specimen, as noticed in reference [25]. Figure 2c shows

the model with the sticking conditions at the contact point. This axisymmetric model takes into account both the axial force (see lower tooling) and the rotational speed (see upper tooling). The friction coefficient and surface pressures between the weld were taken into account. When the temperature is low, the friction stress is calculated using the Coulomb friction law according to the following formulae:

$$\tau_f = -\mu\sigma_n \frac{v_s}{|v_s|} \quad (1)$$

where  $\tau_f$  is the shear friction,  $\mu$  is the friction coefficient,  $\sigma_n$  is the normal stress, and  $v_s$  is the sliding velocity; the negative sign characterizes the opposition between the friction stress. The friction coefficient  $\mu$  can be estimated as follows:

$$\mu = aP^b T^c \exp(dV) \quad (2)$$

where  $P$ ,  $T$  and  $V$  are the axial pressure, temperature and linear velocity, and  $a$ ,  $b$ ,  $c$  and  $d$  are the constants obtained from the experiments.

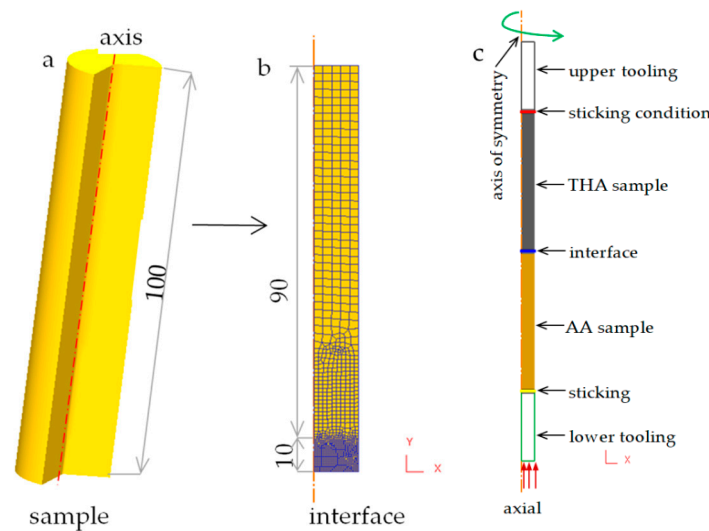


**Figure 2.** Two-dimensional axisymmetric model (a), mesh of the samples (b) and sticking condition (c).

When the temperature is high, the shear friction law is adopted and can be described as follows:

$$\tau_f = -mk \frac{v_s}{|v_s|} \quad (3)$$

where  $k$  is the shear yield stress of the material and  $m$  the friction factor [26].

In this study, to determine an appropriate shear friction, preliminary simulations were carried out. It was found that using a shear friction of 0.175 gave the best results for the given temperatures.

Data regarding the temperature-dependent thermal conductivity, specific heat and emissivity for AA were used; these were obtained from the DEFORM software library. The thermophysical properties of THA were taken from the ASM Handbook [2]. The properties of both materials for the simulation model are presented in Table 2.

The viscoplastic behavior of the materials is characterized by the temperature, flow stress and strain rate, and was obtained from the literature [2].

Figure 3 shows the flow stress for the aluminum (Figure 3a) alloy and tungsten composite (Figure 3b) at a strain of  $\epsilon = 0.1$  during deformation. The convective heat transfer coefficient was assumed to be  $10 \text{ W}/(\text{m}^2 \text{ K})$ . The ambient temperature and initial temperature were set to  $20 \text{ }^\circ\text{C}$ .

**Table 2.** Thermophysical properties of the materials.

Material	AA	THA
Density (kg/m <sup>3</sup> )	2690	18,000
Young modulus (GPa)	69	385
Poisson ratio	0.33	0.28
Thermal expansion (1/C)	$2.2 \times 10^{-5}$	$5.2 \times 10^{-6}$
Specific heat (J/kg K)	528	134
Thermal conductivity (W/m K)	135	90
Melting point (°C)	640	2173

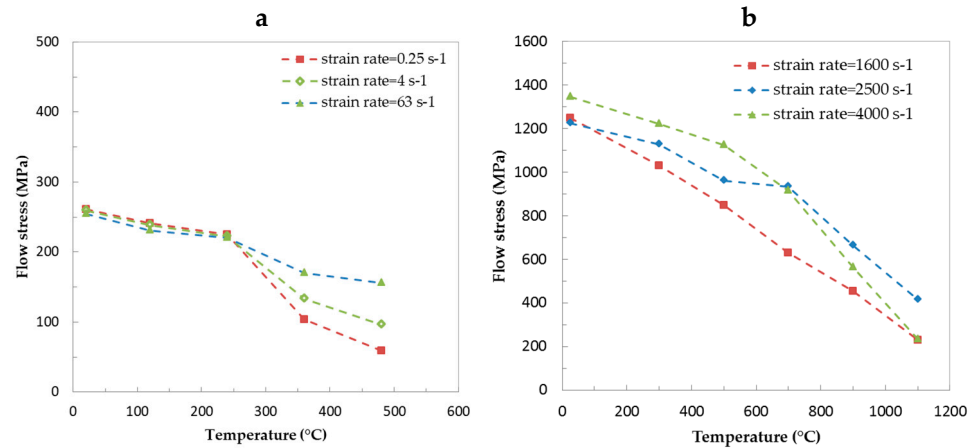


**Figure 3.** The flow stress of AA (a) and THA (b) at strain  $\epsilon = 0.1$  during deformation.

### 3. Results and Discussion

#### 3.1. Temperature Distribution

The temperature field distributions during the friction stage of the FRW process of THA to AA are presented in Figure 4. As can be seen in the graphs, the friction welding process begins in the places most distant from the axis of the cylindrical samples. This is where the highest peripheral speed occurs, where the material becomes plasticized as a result of increasing temperature. Figure 4a shows a relatively rapid increase in temperatures during the friction period of the samples. After 3 s, the temperature on the surface reached 278 °C. After another 3 s, the temperature almost doubled (Figure 4b). It is likely that the high-temperature zone widens from the weld line due to heat conduction within the specimen. As can be seen in Figure 4c, no significant plastic deformation or flash formation occurred during the friction phase.

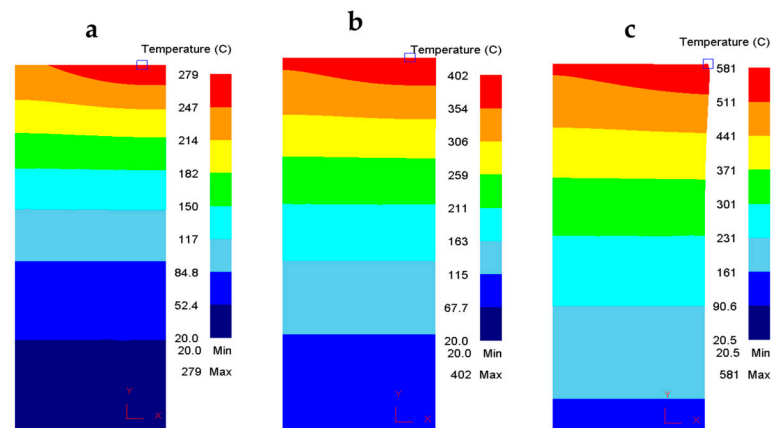


**Figure 4.** Distributions of temperature fields in aluminum alloy during the friction period: (a) 3 s (b) 6 s (c) 9.5 s. (FF = 12.5 kN, n = 1450 rpm, and UF = 50 kN).

The maximum interface temperature of 581 °C for the friction weld was achieved in a time of 9.6 s (Figure 5).

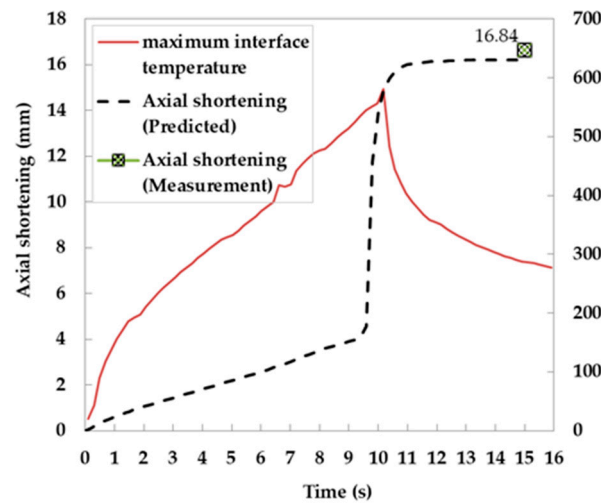


Figure 5. Maximum temperature distribution and axial shortening of welded materials during friction welding.

Figure 6 shows the temperature distribution fields of the weld zone during the upsetting stage of the welding process. As can be seen in Figure 5, after reaching the maximum value, the temperature drops rapidly to 280 °C within a few seconds during the forging stage (see Figure 6a–c).

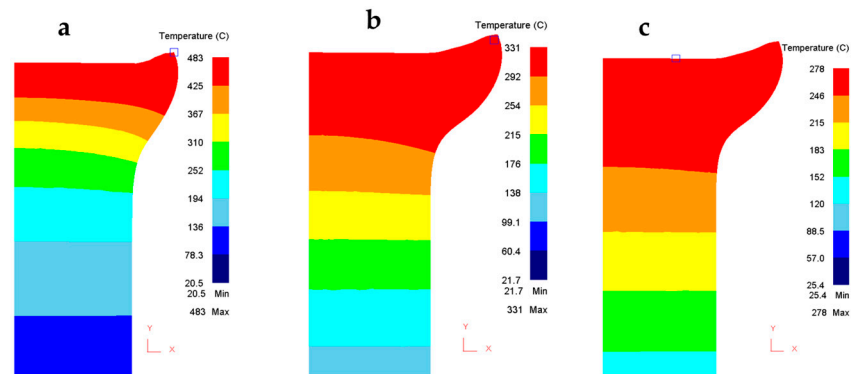
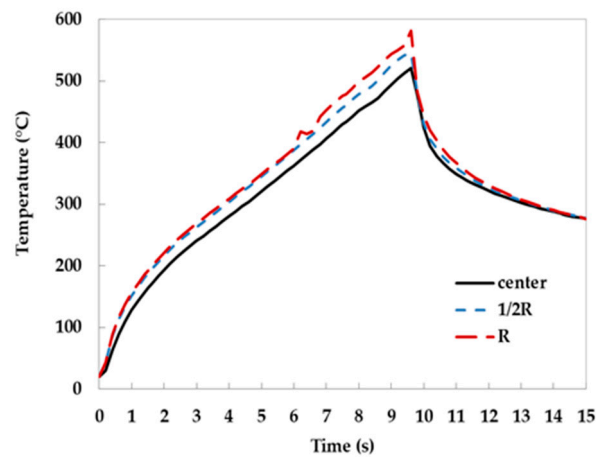


Figure 6. Temperature distribution of weld zone during the upsetting stage of the FRW process of THA/AA dissimilar alloys: (a) 11 s, (b) 13 s and (c) 15 s. (FF = 12.5 kN, n = 1450 rpm, and UF = 50 kN).

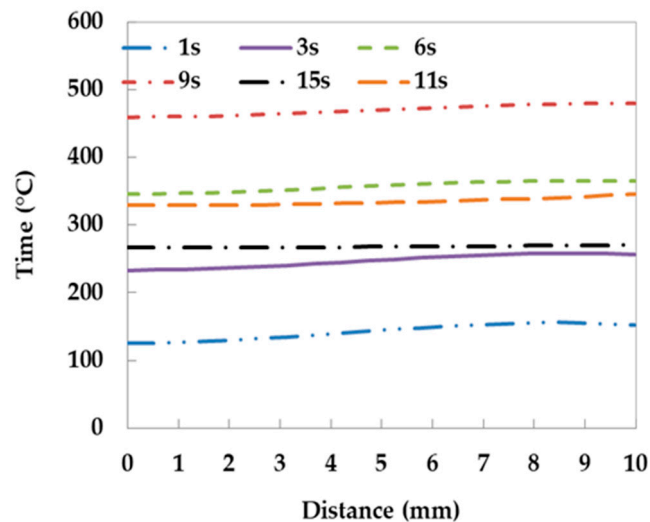
It is found that the weld flash begins from 9.6 s to 15 s and that the largest flash is obtained after the upsetting process (Figure 6c). The plastic deformation that accompanies this welding phase causes the significant shortening of the aluminium alloy (Figure 5). It can be seen that the maximum axial shortening of 16.8 mm is achieved during this stage.

Figure 7 shows the thermal history of the weld interface for various positions. It can be seen that the temperature on the outer surface is the highest, while that on the axis has the lowest value. The highest temperature values were recorded at the welding time of 9.5 s. For all measurement locations, the nature of the temperature distribution is similar. This is because the temperature increases linearly with the increasing friction time. After obtaining the highest value, the temperature drops rapidly, but on the outer surface, this reduction is the smallest.



**Figure 7.** Thermal curves in the weld interface.

The radial distribution of temperature for various durations is obtained via simulation in Figure 8.



**Figure 8.** The radial temperature distribution at different times.

It can be noted that an appropriate welding time is required to reach the friction welding temperature of the welding process for specific parameters. The radial temperature was measured for the following welding parameters: rotational speed = 152 rad/s, friction force = 12.5 kN, upsetting time and force of 5 s and 50 kN, respectively. Similar results were obtained for other welding parameters.

### 3.2. Experimental Validation

#### 3.2.1. Experimental Temperature Validation

The typical simulation result is obtained under a friction force, upsetting force, friction time, upsetting time and rotating speed of 12.5 kN, 50 kN, 9 s, 5 s and 1450 rpm, respectively. The computed and measured temperatures on the AA side are plotted for comparison. As shown in Figure 9, the thermocouples were placed in the middle of the radius and the axis of the joint at distances of 20, 25 and 30 mm from the welding line (see Figure 1b). Initially, the thermocouples were positioned close to the weld interface, but they were consumed during the forging phase of the welding process. Due to the continuous 'upset' (axial shortening) of the specimens during welding, it is naturally difficult to place thermocouples that can record exact temperatures. Consequently, the first thermocouple was located about 20 mm

away from the weld interface. The thermocouple wires were stuck onto the surfaces of the measuring specimen with high-temperature-resistant glue.

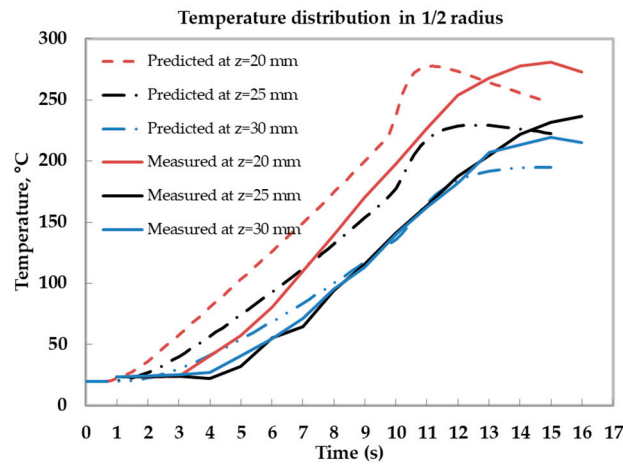


**Figure 9.** Predicted and measured temperature in AA side at the 1/2 radial position and at a distance of 0, 20, 25 and 30 mm from the original weld interface.

Figure 9 shows the similar characteristics of the temperature course during the heating of the materials. The predicted temperature values are slightly higher than the temperature values obtained from the thermocouple readings. According to the authors [27,28], these differences could be a result of reading the delay times and the time constant of the thermocouples.

Figure 10 shows the validation of the temperature at half of the sample radius.

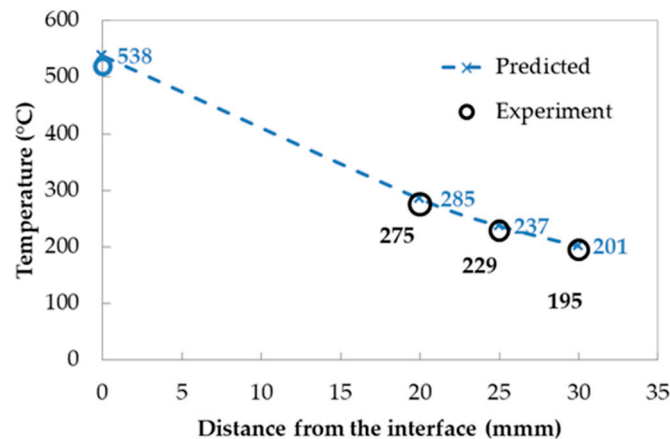


**Figure 10.** Validation of maximum temperature at the 1/2 radial position.

As can be seen from Figure 10, the predicted temperature is slightly higher than the temperature obtained by the experiment at distances of 20, 25 and 30 mm from bond line. The accuracy of the predicted temperature is quite good. The temperature results indicate small deviations of 3.6%, 3.5% and 3% for distances of 20, 25 and 30 mm from the interface. The maximum temperature near the welding point reached 538 °C in 1/2 of the sample radius for 9.5 s (Figure 10). Despite the plastic deformation of the material, this temperature did not reach the melting point of the aluminium alloy.

### 3.2.2. Macroscopic Morphology Validation

During the welding process, the plastic deformation of the joined materials occurs. The result of this process is the shortening of the soft metal and the formation of a weld flash. After completing the welding process, both the weld flash and the length of the

samples were measured. A comparison of the macroscopic morphology of the friction welds using numerical simulation is shown in Figure 11.

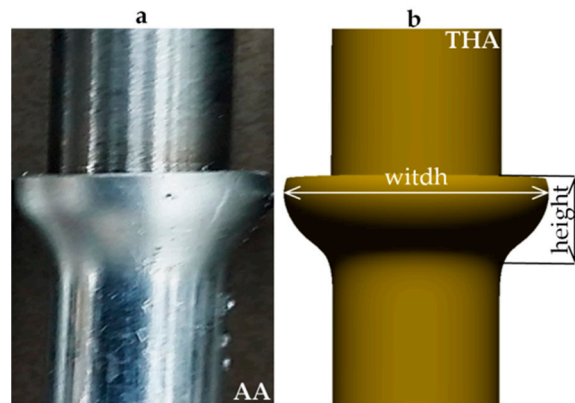


**Figure 11.** Comparison of the macroscopic morphology of the friction welds (a) and numerical simulation (b).

It can be seen from Figure 11 that the flash morphologies are nearly identical. A quantitative comparison of the flash dimensions obtained via the experiment and numerical simulations is shown in Table 3. Axial shortening is also selected for comparison.

**Table 3.** Comparison of flash dimension and axial shortening.

	Flash Dimensions		Shortening, mm
	Width, mm	Height, mm	
Measurement	33.66	16.84	16.61
Predicted	32.16	16.34	16.22

The results indicate very small deviations of 4.45%, 2.96%, and 2.34% in the flash width, flash height and axial shortening of the friction welds.

### 3.3. Effect of Friction Force on Interface Temperature

Figure 12 shows the influence of the frictional pressure force on the temperature in the joint during welding. The maximum temperature was obtained for the highest friction force. By increasing the friction force, the temperature rises and reaches the maximum interface temperature at a time of 7.5 s for all axial forces.

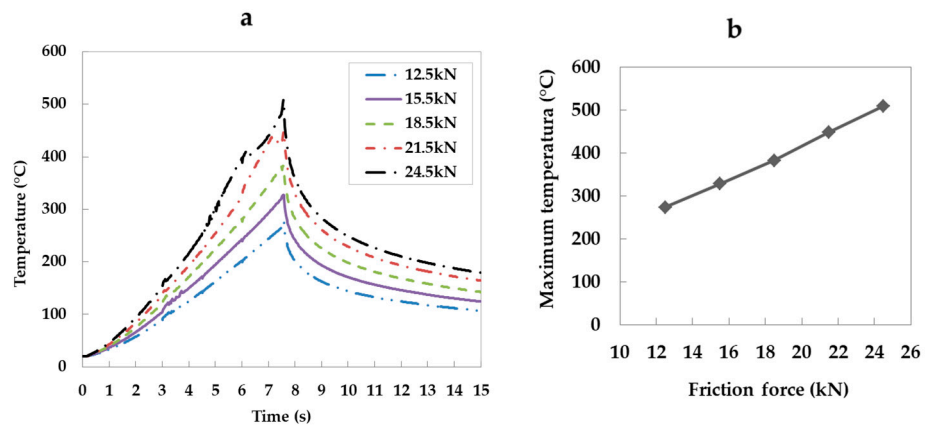


**Figure 12.** Influence of friction force on temperature during welding: temperature and various friction force in time (a), friction force and maximum temperature (b).

### 3.4. Effect of Friction Force on Axial Shortening

Figure 13 shows the effect of the friction force on axial shortening for friction forces of 12.5, 15.5, 18.5, 21.5 and 24.5 kN. It is clear that during the friction phase between materials, axial shortening takes place. As the friction time increases (from 12.5 to 18 kN), the axial shortening of the samples increases linearly. During the upsetting phase, it can be seen that a logarithmic shortening of the material takes place when using axial forces from 18.5 to 25 kN (Figure 13b).

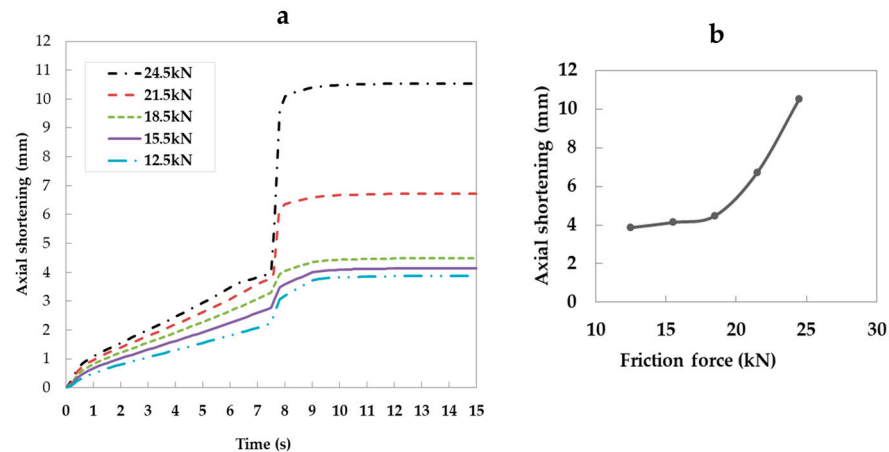


**Figure 13.** Effect of friction force on the axial shortening of the specimen: axial shortening and various friction force in time (a), friction force and axial shortening (b).

For all applied forces, the maximum shortening of the samples did not exceed 4 mm at the end of the friction phase. After this time, plastic deformation occurred and a weld flash was formed. This process took a few seconds. A rapid loss of material occurred after applying the upsetting force for a welding time of 8 s. The maximum material shortening was 3.5 mm for a friction force of 12 kN. Doubling the friction force shortened the material by an additional 7 mm (Figure 13b). Moreover, from Figure 13a, it can be seen that the forging period had a minimal effect on the upset. The axial shortening is almost unchanged throughout this stage. A similar observation reported in the references [29–31].

### 3.5. Effective Stress Distribution

Figure 14 shows the effective stress evolution at the three various positions of the weld interface.

As can be seen in Figure 14a, the effective stresses for the three positions during the friction period are relatively small. These stresses at the beginning of the friction process are 25, 45 and 50 MPa for the surface, axis, and 1/2 of the radius, respectively. The effective stresses on the sample surface are the smallest because no relative motion happens and only slight friction stress exists in this place [32]. The stresses gradually decrease and reach a value of 20 MPa at the end of the friction stage (Figure 14c) for all positions. At the beginning of the forging stage (Figure 14d), there is a sudden increase in stress, achieving 60 MPa and 80 MPa on the surface and in the axis of the joint, respectively. Constant effective stress takes place during forging from 10 to 12 s (Figure 14e). After stopping the welding process, the stress drops to zero. Moreover, it can be seen that the effective stress is lower in the periphery joint compared to the interior of the weld interface. According to the authors of reference [26], the friction stress is proportional to the shear yield strength.

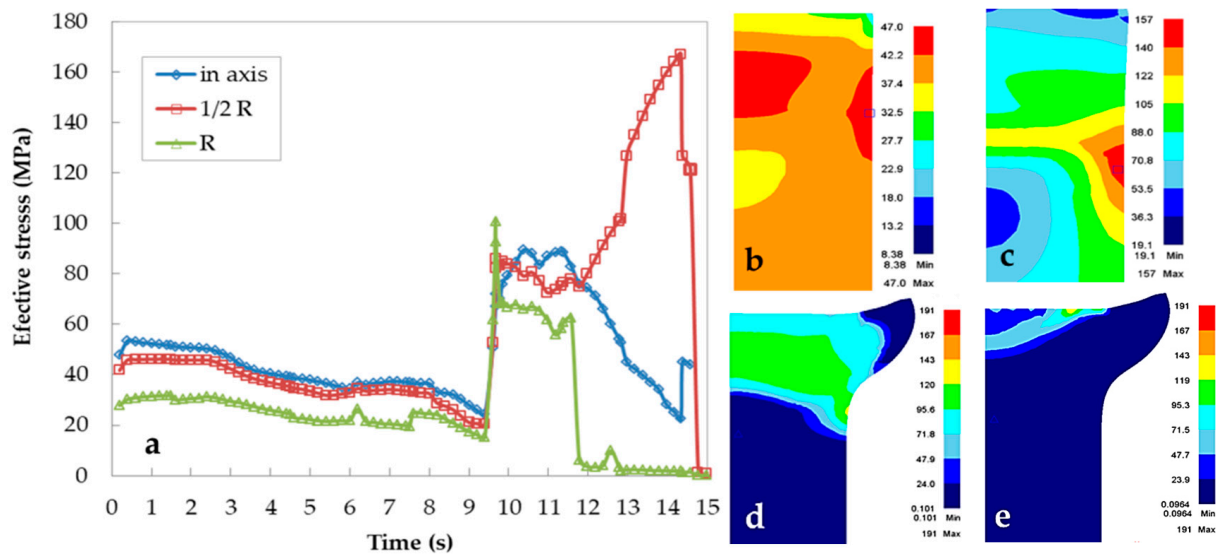


**Figure 14.** Predicted effective stress in the aluminum alloy specimen for various radial positions at the weld interface; effective stress flow during welding time (a), friction stage (b,c), forging stage (d,e).

#### 4. Conclusions

An experimental and FEM simulation study of the CDFW process of a THA with an aluminum alloy is presented. The temperature distributions, effective stress, flash dimensions and axial shortening are calculated on un-rotated friction-welded aluminium parts. An increase in the friction force causes an increase in temperature during the friction period of the samples. It can predict the shape of the flash with a high degree of accuracy. The predicted temperature was slightly higher than the temperature obtained in the experiment. The maximum interface temperature of 581 °C is below the melting temperature of the aluminum sample. The results indicate very small deviations of 4.45%, 2.96%, and 2.34% in the flash width, flash height and axial shortening of the friction welds. With an increasing friction force, axial shortening increases exponentially. The effective stresses on the sample surface are the smallest because no relative motion occurs and only slight friction stress exists in this place.

**Author Contributions:** Conceptualization and Methodology, R.W. and A.S.; Software, R.W.; Modelling and optimization, R.W.; Validation, R.W. and A.S.; Formal analysis, R.W.; Investigation, R.W., A.S. and P.S.; Resources, R.W.; Writing-original draft preparation, R.W.; Writing-review and editing, R.W.; Visualization, R.W.; Supervision, R.W. All authors have read and agreed to the published version of the manuscript.

**Funding:** This research received no external funding.

**Institutional Review Board Statement:** Not applicable.

**Informed Consent Statement:** Not applicable.

**Data Availability Statement:** Data are contained within the article.

**Acknowledgments:** The authors wish to thank Mieczysław Kaczorowski from the Faculty of Mechanics of Institute of Mechanics and Design, Warsaw University of Technology, for his valuable suggestions.

**Conflicts of Interest:** The authors declare no conflicts of interest.

#### References

1. American Welding Society. Specifications and standards. In *Recommended Practice for Friction Welding*; American Welding Society: Miami, FL, USA, 1989.
2. Withers, P.J.; Preuss, M. *Simulation of Rotational Welding Operations*; Metals Process Simulation, ASM Handbook; ASM International: Materials Park, OH, USA, 2010; Volume 22B.

3. Vill, V.I. *Friction Welding of Metals*; AWS: New York, NY, USA, 1962.
4. Rich, T.; Roberts, R. Thermal Analysis for Basic Friction Welding. *Met. Constr. Br. Weld. J.* **1971**, *3*, 93–98.
5. Imshennik, K.P. Heating in Friction Welding. *Weld. Prod.* **1973**, *20*, 76–79.
6. Cheng, C.J. Transient temperature distribution during friction welding of two similar materials in tubular form. *Weld. J.* **1963**, *12*, 223–240.
7. Healy, J.; McMullan, D.J.; Bahrani, A.S. Analysis of Frictional Phenomena in Friction Welding of Mild Steel. *Wear* **1976**, *37*, 279–289. [[CrossRef](#)]
8. Kinley, W. Inertia Welding: Simple in Principle and Application. *Weld. Met. Fabr.* **1979**, 585–589.
9. Murti, K.; Sundaresan, G.; Parameter, S. Optimization in Friction Welding Dissimilar Materials. *Met. Constr. Br. Weld. J.* **1983**, *15*, 331–335.
10. Kleiber, M.; Służalec, A. Finite element analysis of heat flow in friction welding. *Eng. Trans.* **1984**, *32*, 107–113.
11. Służalec, A. Thermal Effects in Friction Welding. *Int. J. Mech. Sci.* **1990**, *32*, 467–478. [[CrossRef](#)]
12. Służalec, A. Solution of thermal problems in friction welding. *Int. J. Heat Mass Transf.* **1993**, *36*, 1583–1587. [[CrossRef](#)]
13. Sahin, Z.; Yilbas, B.S.; Al-Garni, A.Z. Friction welding of Al–Al, Al–steel, and steel–steel samples. *J. Mater. Eng. Perform.* **1996**, *5*, 89–99. [[CrossRef](#)]
14. Bendzsak, G.J.; North, T.H.; Li, Z. Numerical Model for Steady-State Flow in Friction Welding. *Acta Mater.* **1997**, *45*, 1735–1745. [[CrossRef](#)]
15. Fu, L.; Duan, L. The Coupled Deformation and Heat Flow Analysis by Finite Element Method during Friction Welding. *Weld. Res. Suppl.* **1998**, *77*, 202–207.
16. Alvisé, L.D.; Massoni, E.; Walloe, S.J. Finite Element Modelling of the Inertia Friction Welding Process between Dissimilar Materials. *J. Mater. Process. Technol.* **2002**, *125*, 387–391.
17. Balasubramanian, V.; Li, Y.; Stotler, T.; Crompton, J.; Soboyejo, A.; Katsube, N.; Soboyejo, W.A. New Friction Law for the Modelling of Continuous Drive Friction Welding: Applications to 1045 Steel Welds. *Mater. Manuf. Process.* **1999**, *14*, 845–860. [[CrossRef](#)]
18. Zimmerman, J.; Włosiński, W.; Lindemann, Z.R. Thermo-mechanical and diffusion modelling in the process of ceramic-metal friction welding. *J. Mater. Process. Technol.* **2009**, *209*, 1644–1653. [[CrossRef](#)]
19. Ambroziak, A. Temperature distribution in friction welded joints of dissimilar refractory metals. *Adv. Manuf. Sci. Technol.* **2002**, *26*, 39–54.
20. Maalekian, M.; Kozeschnik, E.; Brantner, H.P.; Cerjak, H. Comparative analysis of heat generation in friction welding of steel bars. *Acta Mater.* **2008**, *56*, 2843–2855. [[CrossRef](#)]
21. Xiong, J.T.; Li, J.L.; Wei, Y.N.; Zhang, F.S.; Huang, W.D. An analytical model of steady-state continuous drive friction welding. *Acta Mater.* **2013**, *61*, 1662–1675. [[CrossRef](#)]
22. Winiczenko, R.; Goroch, O.; Krzyńska, A.; Kaczorowski, M. Friction welding of tungsten heavy alloy with aluminium alloy. *J. Mater. Process. Technol.* **2017**, *246*, 42–55. [[CrossRef](#)]
23. Winiczenko, R.; Kaczorowski, M.; Krzyńska, A.; Goroch, O.; Skibicki, A.; Skoczylas, P. TEM Microstructure, Mechanical Properties and Temperature Estimation in the 5XXX Series Al–Mg–Si Aluminum Alloy with W–Ni–Fe Tungsten Composite Friction-Welded Joints. *Materials* **2022**, *15*, 1162. [[CrossRef](#)]
24. Perovic, N.L.; Maglic, K.D.; Stanimirovic, A.M.; Vukovic, G.S. Transport and calorimetric properties of AISI 321 by pulse thermal diffusivity and calorimetric techniques. *High Temp. High Press* **1995**, *1*, 53–58. [[CrossRef](#)]
25. Hazman, S.; Ismail, A.I.M.; Endri, R.; Zainal, A.H. Mechanical evaluation and thermal modeling of friction welding of mild steel and aluminium. *J. Mater. Process. Technol.* **2010**, *210*, 1209–1216.
26. Zang, Q.Z.; Zhang, L.W.; Liu, W.W.; Zhang, V.G.; Qu, S. 3D rigid viscoplastic FE modelling of continuous drive friction welding process. *Sci. Technol. Weld. Join.* **2006**, *11*, 737–743. [[CrossRef](#)]
27. Shailesh, K.; Singh, K.; Chattopadhyay, G.; Phanikumar, K.; Dutta, P. Experimental and numerical studies on friction welding of thixocast A356 aluminum alloy. *Acta Mater.* **2014**, *73*, 177–185.
28. Le, W.S.; Xiea, G.L.; Lin, C.F. The strain rate and temperature dependence of the dynamic impact response of tungsten composite. *Mater. Sci. Eng.* **1998**, *257*, 256–267. [[CrossRef](#)]
29. Li, W.; Wang, F. Modeling of continuous drive friction welding of mild steel. *Mater. Sci. Eng. A.* **2011**, *528*, 5921–5926. [[CrossRef](#)]
30. Geng, P.; Qin, G.; Zhou, J. Numerical and experimental investigation on friction welding of austenite stainless steel and middle carbon steel. *J. Manuf. Process.* **2019**, *47*, 83–97. [[CrossRef](#)]
31. Wang, F.F.; Li, W.Y.; Li, J.L.; Vairis, A. Process parameter analysis of inertia friction welding nickel-based superalloy. *Int. J. Adv. Manuf. Technol.* **2014**, *71*, 1909–1918. [[CrossRef](#)]
32. Nu, H.; Le, T.; Minh, L.; Loc, N. A Study on Rotary Friction Welding of Titanium Alloy (Ti6Al4V). *Adv. Mater. Sci. Eng.* **2019**, *2019*, 4728213.

**Disclaimer/Publisher’s Note:** The statements, opinions and data contained in all publications are solely those of the individual author(s) and contributor(s) and not of MDPI and/or the editor(s). MDPI and/or the editor(s) disclaim responsibility for any injury to people or property resulting from any ideas, methods, instructions or products referred to in the content.